

Supplementary Information to accompany

Modulating the electronic properties of divalent lanthanoid complexes with subtle ligand tuning

*Moya A. Hay, Robert W. Gable, Colette Boskovic**

School of Chemistry, University of Melbourne, Parkville, Victoria 3010, Australia

E-mail: c.boskovic@unimelb.edu.au

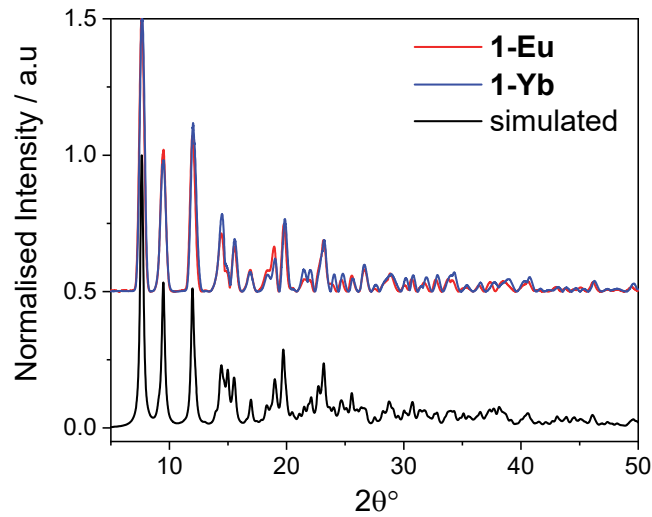


Fig. S1 Experimental PXRD patterns for **1-Eu** and **1-Yb** (300 K) vs simulated pattern from crystal structure of **1-Eu** (100 K).

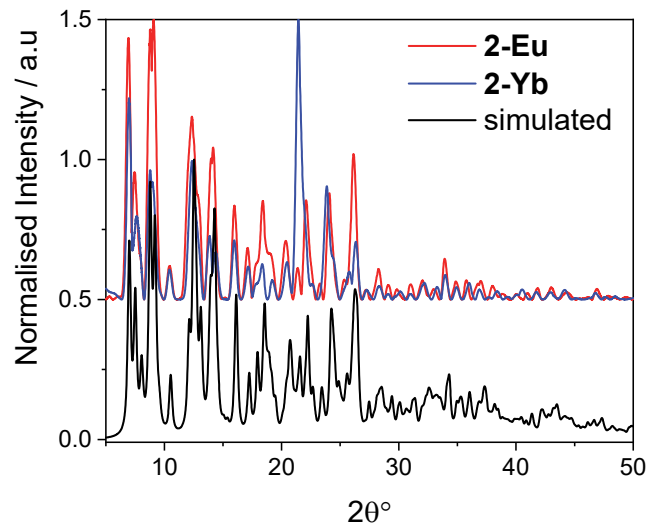


Fig. S2 Experimental PXRD patterns for **2-Eu** and **2-Yb** (300 K) vs simulated pattern from crystal structure of **2-Eu** (100 K).

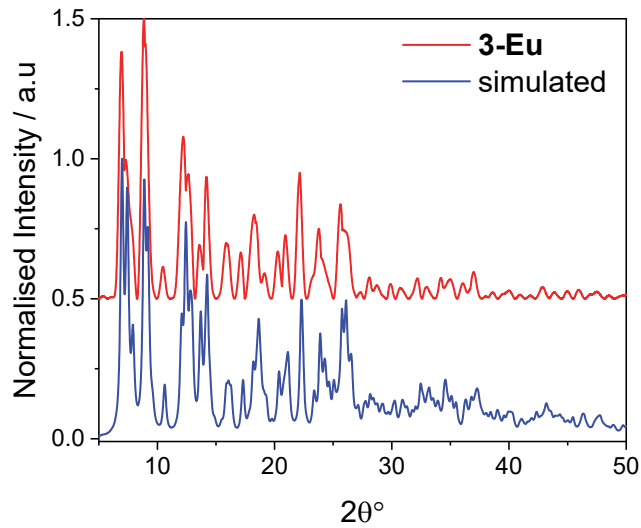


Fig. S3 Experimental PXRD pattern for **3-Eu** (300 K) vs simulated pattern from crystal structure of **3-Eu** (100 K).

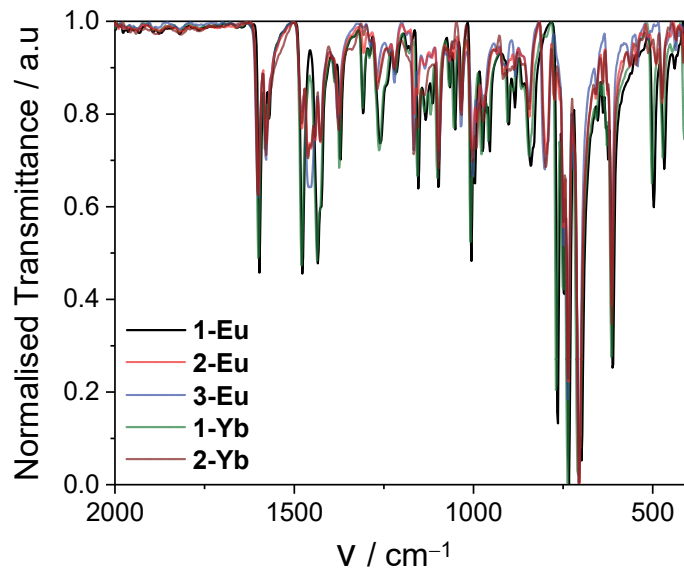


Fig. S4 Solid state infrared spectra (ATR) for compounds **1-Ln**, **2-Ln** and **3-Eu**, demonstrating the similar chemical composition of the series.

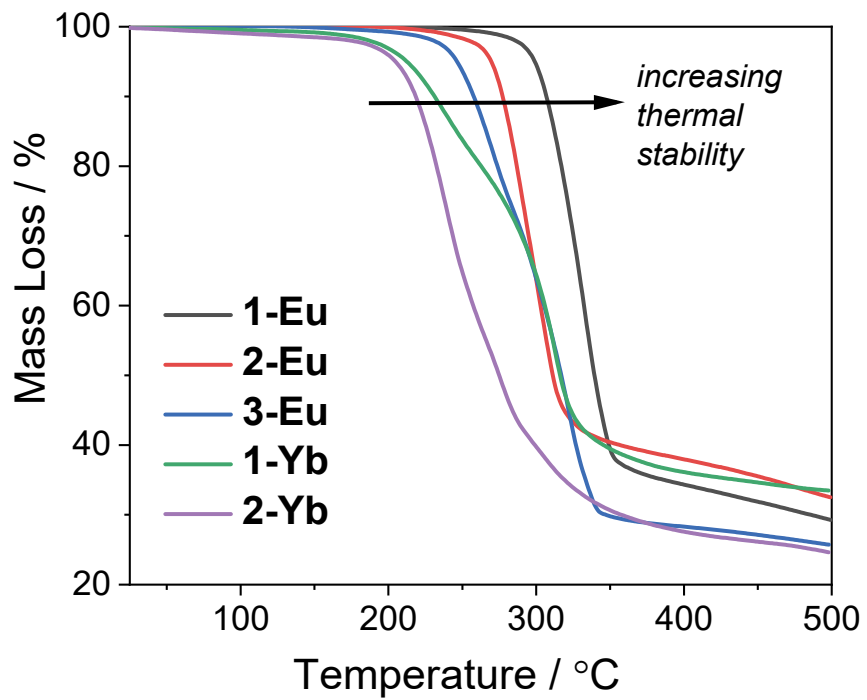


Fig. S5 Thermogravimetric analyses (TGA) in the range 25 - 500°C under N₂ flow for **1-Ln**, **2-Ln**, **3-Eu**, demonstrating relative thermal stability in the solid state.

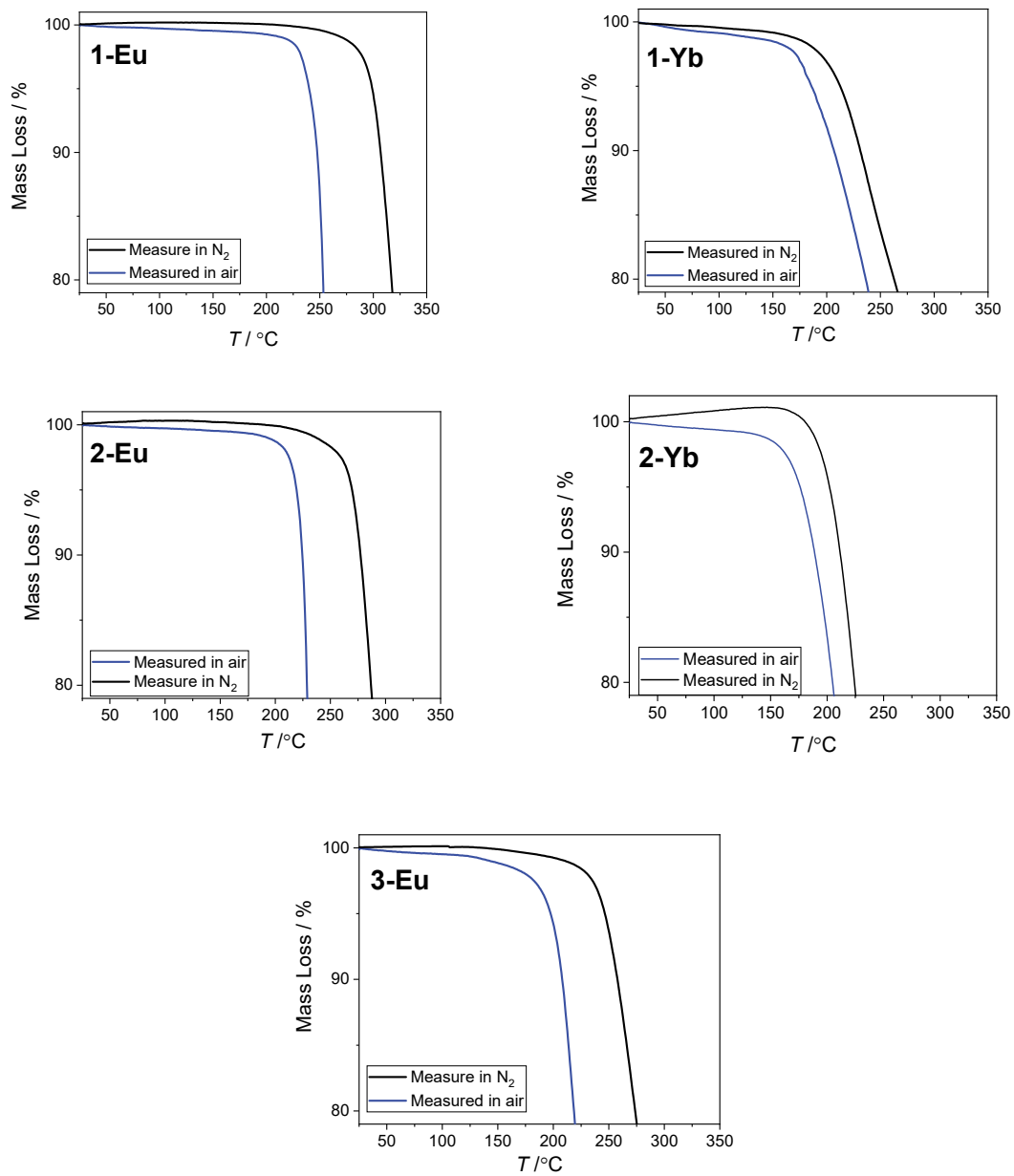


Fig. S6 Comparison of the thermogravimetric analysis (TGA) conducted under N₂ vs air between 25 - 350°C for **1-Ln**, **2-Ln**, **3-Eu**.

Additional Crystal Refinement and Solution Information

For compounds **2-Eu**, **2-Yb** and **3-Eu** it was necessary to model disorder present in the coordinate Me_ntpa ligands, which was evident in residual electron density and atomic displacement parameters. In all cases, the E-statistics suggested a non-centrosymmetric space group, while the Cumulative Intensity Distribution suggested the space group was twinned acentric. A satisfactory solution was obtained in the centrosymmetric space group P-1 (SHELXT). The carbon atoms around the tertiary nitrogen atoms were disordered, giving rise to two different conformations of the ligand. Refinement was carried out with the molecule distributed over two different conformations such that the atoms of each pyridine group and the two attached carbon atoms were restrained to be coplanar, the geometry of the two components were restrained to be equal and the displacement parameters of the two components of each atom were constrained to be equal the relative occupancies of the components was allowed to refine. The final refinement gave final occupancy factors of 0.553:0.447 for **2-Eu**, 0.570:0.430 for **2-Yb**, and 0.641:0.359 for **3-Eu**. There were numerous electron density peaks around the BPh₄⁻ anion for **2-Eu** and **2-Yb**, indicating disorder. The anion was refined as being disordered over two positions; the final occupancy factors were 0.773:0.227 for **2-Eu** and 0.570:0.430 for **2-Yb**. No disorder was apparent for the BPh₄⁻ anion for **3-Eu**. A second form of disorder was evident in the methyl groups of the Me₂tpa ligand for **2-Eu** and **2-Yb**. The difference map showed that the two methyl carbon atoms attached to the pyridine rings were almost equally distributed over three possible sites. Refinements was carried out with the occupancy factors of the methyl atoms being 2/3 of the occupancy of the ring atoms.

Table S1 Crystallographic data and structure refinement parameters for compounds **1-Eu** and **1-Yb**.

	1-Eu	1-Yb
Empirical formula	C ₈₄ H ₇₆ B ₂ EuN ₈	C ₈₄ H ₇₆ B ₂ N ₈ Yb
Formula weight	1371.10	1392.18
Temperature (K)	100	100
Crystal system	monoclinic	monoclinic
Space group	P2 ₁ /n	P2 ₁ /n
<i>a</i> (Å)	12.400(3)	12.31789(11)
<i>b</i> (Å)	14.478(3)	14.28779(11)
<i>c</i> (Å)	19.954(4)	19.67463(15)
α (°)	90	90
β (°)	103.31(3)	103.2045(8)
γ (°)	90	90
Volume (Å ³)	3486.1(13)	3371.10(5)
<i>Z</i>	2	2
ρ_{calc} (g/cm ³)	1.306	1.372
μ (mm ⁻¹)	0.951	2.970
F(000)	1418.0	1432.0
Crystal size (mm ³)	0.07 × 0.06 × 0.02	0.07 × 0.06 × 0.04
Radiation	synchrotron ($\lambda = 0.71073$)	Cu K α ($\lambda = 1.54184$)
2θ range for data collection (°)	3.508 to 64.634	7.72 to 154.21
Index ranges	-16 ≤ <i>h</i> ≤ 16, -18 ≤ <i>k</i> ≤ 18, -29 ≤ <i>l</i> ≤ 29	-14 ≤ <i>h</i> ≤ 15, -18 ≤ <i>k</i> ≤ 17, -20 ≤ <i>l</i> ≤ 24
Reflections collected	63179	41583
Independent reflections	10464 [$R_{\text{int}} = 0.0954$, $R_{\text{sigma}} = 0.0574$]	6994 [$R_{\text{int}} = 0.0389$, $R_{\text{sigma}} = 0.0257$]
Data/restraints/parameters	10464/0/431	6994/0/430
Goodness-of-fit on F^2	1.083	1.121
Final <i>R</i> indexes [$I \geq 2\sigma(I)$]	$R_1 = 0.0385$, $wR_2 = 0.1118$	$R_1 = 0.0271$, $wR_2 = 0.0707$
Final <i>R</i> indexes [all data]	$R_1 = 0.0411$, $wR_2 = 0.1158$	$R_1 = 0.0327$, $wR_2 = 0.0733$
Largest diff. peak/hole / e Å ⁻³	0.78/-0.85	1.50/-0.82

Table S2 Crystallographic data and structure refinement parameters for compounds **2-Eu**, **2-Yb**, and **3-Eu**.

	2-Eu	2-Yb	3-Eu
Empirical formula	$\text{EuC}_{88}\text{H}_{82}\text{B}_2\text{N}_8$	$\text{YbC}_{88}\text{H}_{82}\text{B}_2\text{N}_8$	$\text{EuC}_{90}\text{H}_{88}\text{B}_2\text{N}_8$
Formula weight	1425.19	1446.27	1455.26
Temperature (K)	100	100	100
Crystal system	triclinic	triclinic	triclinic
Space group	P-1	P-1	P-1
<i>a</i> (Å)	11.0546(2)	11.04793(17)	10.940(3)
<i>b</i> (Å)	13.4390(2)	13.51325(19)	13.650(3)
<i>c</i> (Å)	14.6816(2)	14.7018(2)	14.736(4)
α (°)	102.9670(10)	103.4083(14)	104.24(3)
β (°)	111.4020(10)	111.5188(13)	110.37(3)
γ (°)	108.5710(10)	109.1372(13)	108.29(3)
Volume (Å ³)	1775.86(5)	1767.44(5)	1795.9(9)
<i>Z</i>	1	1	1
ρ_{calc} (g/cm ³)	1.333	1.359	1.346
μ (mm ⁻¹)	6.725	2.853	0.928
F(000)	739.0	764.0	757.0
Crystal size (mm ³)	0.151 × 0.116 × 0.033	0.138 × 0.098 × 0.02	0.05 × 0.05 × 0.05
Radiation	Cu Kα ($\lambda = 1.54184$)	CuKα ($\lambda = 1.54184$)	synchrotron ($\lambda = 0.71073$)
2θ range for data collection (°)	7.01 to 154.264	7.054 to 155.372	3.216 to 64.3
Index ranges	-13 ≤ <i>h</i> ≤ 12, -16 ≤ <i>k</i> ≤ 16, -17 ≤ <i>l</i> ≤ 18	-13 ≤ <i>h</i> ≤ 12, -16 ≤ <i>k</i> ≤ 17, -18 ≤ <i>l</i> ≤ 17	-14 ≤ <i>h</i> ≤ 14, -17 ≤ <i>k</i> ≤ 17, -21 ≤ <i>l</i> ≤ 21
Reflections collected	22958	23658	32556
Independent reflections	7238 [$R_{\text{int}} = 0.0478$, $R_{\text{sigma}} = 0.0424$]	7230 [$R_{\text{int}} = 0.0541$, $R_{\text{sigma}} = 0.0487$]	9390 [$R_{\text{int}} = 0.0373$, $R_{\text{sigma}} = 0.0346$]
Data/restraints/parameters	7238/196/639	7230/262/645	9390/136/563
Goodness-of-fit on F^2	1.060	1.058	1.064
Final <i>R</i> indexes [$I \geq 2\sigma(I)$]	$R_1 = 0.0429$, $wR_2 = 0.1069$	$R_1 = 0.0490$, $wR_2 = 0.1230$	$R_1 = 0.0355$, $wR_2 = 0.0927$
Final <i>R</i> indexes [all data]	$R_1 = 0.0435$, $wR_2 = 0.1077$	$R_1 = 0.0601$, $wR_2 = 0.1366$	$R_1 = 0.0358$, $wR_2 = 0.0930$
Largest diff. peak/hole / e Å ⁻³	0.56/-0.73	1.41/-0.71	2.02/-1.77

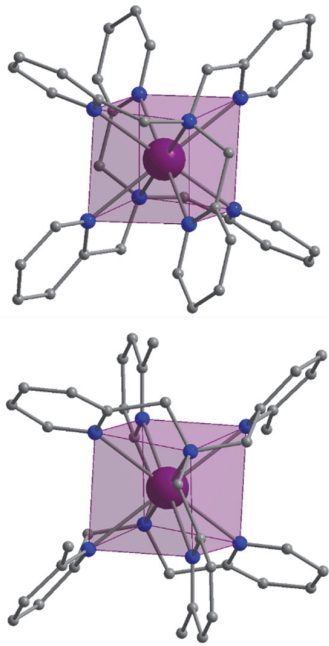


Fig. S7 Molecular structures of Yb complexes in **1-Yb** (top) and **2-Yb** (bottom), highlighting approximate cubic coordination. Hydrogen atoms and counterions have been omitted for clarity. Color code as per Fig 1 with Yb (violet).

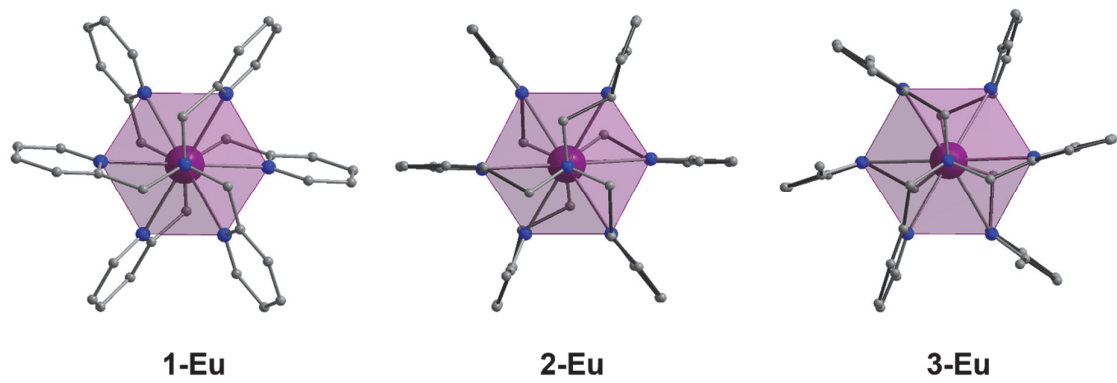


Fig. S8 Molecular structures of Eu complexes in **1-Eu**, **2-Eu** and **3-Eu** viewed along N(amine)···N(amine) axis to highlight staggered arrangements of ligands. Color code as per Fig 1.

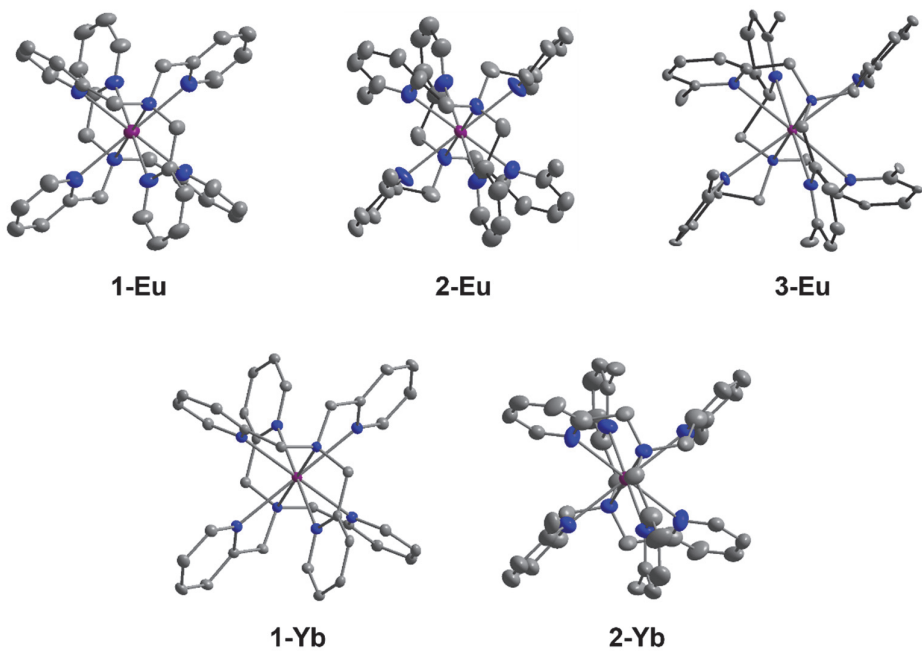


Fig. S9 Molecular structures of metal complexes depicting atomic displacement parameters via thermal ellipsoids at the 30 % probability level. Hydrogen atoms have been omitted for clarity. Color code as per Figs 1 and S7.

Table S3 Shape distortion parameters determined for various 8-coordination geometries for **1-Ln**, **2-Ln** and **3-Eu**.

	1-Eu	2-Eu	3-Eu	1-Yb	2-Yb
Cu-8 ^a	1.527	1.037	1.087	0.958	0.687
TDD-8 ^b	9.334	8.897	8.933	8.815	8.574
SAPR-8 ^c	12.31	11.90	11.93	11.81	11.59
HPBY-8 ^d	7.099	6.984	7.040	7.209	7.175
HPY-8 ^e	27.5	27.98	26.12	27.97	28.28
OP-8 ^f	33.32	34.47	34.47	34.23	34.94
JGBF-8 ^g	16.71	16.84	17.07	16.99	17.06
JETBPY-8 ^h	19.59	21.15	21.84	20.55	22.33
JBTPR-8 ⁱ	13.61	13.45	13.57	13.36	13.26
BTPR-8 ^j	13.05	12.81	12.83	12.80	12.65
JSD-8 ^k	15.49	15.12	15.12	15.01	14.81
TT-8 ^l	2.456	1.972	2.022	1.894	1.627
ETBPY-8 ^m	16.65	17.81	17.95	17.83	18.92

^a CU-8 = cube, ^b TDD-8 = triangular dodecahedron, ^c SAPR-8 = square antiprism, ^d HBPY-8 = hexagonal bipyramid, ^e HPY-8 = heptagonal pyramid, ^f OP-8 = regular octagon, ^g JGBF-8 = johnson gyrobifastigium J26, ^h JETBPY-8 = johnson elongated triangular bipyramid, ⁱ JBTPR-8 = biaugmented trigonal prism J50, ^j BTPR-8 = biaugmented trigonal prism, ^k JSD-8 = snub diphenoïd J84, ^l TT-8 = triakis tetrahedron, ^m ETBPY-9 = elongated trigonal bipyramid in *SHAPE* 2.1.^{1,2}

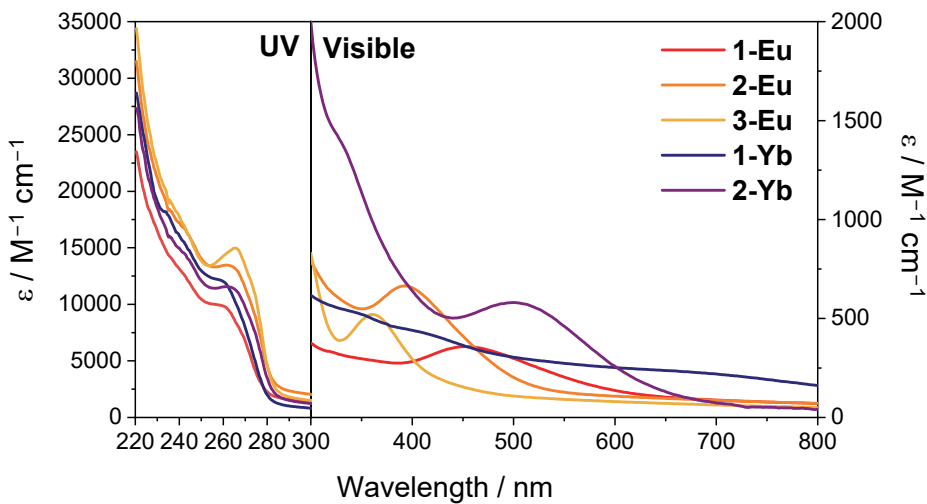


Fig. S10 UV (left) and visible (right) range spectra for MeCN solutions of compounds **1-Ln**, **2-Ln**, and **3-Ln**.

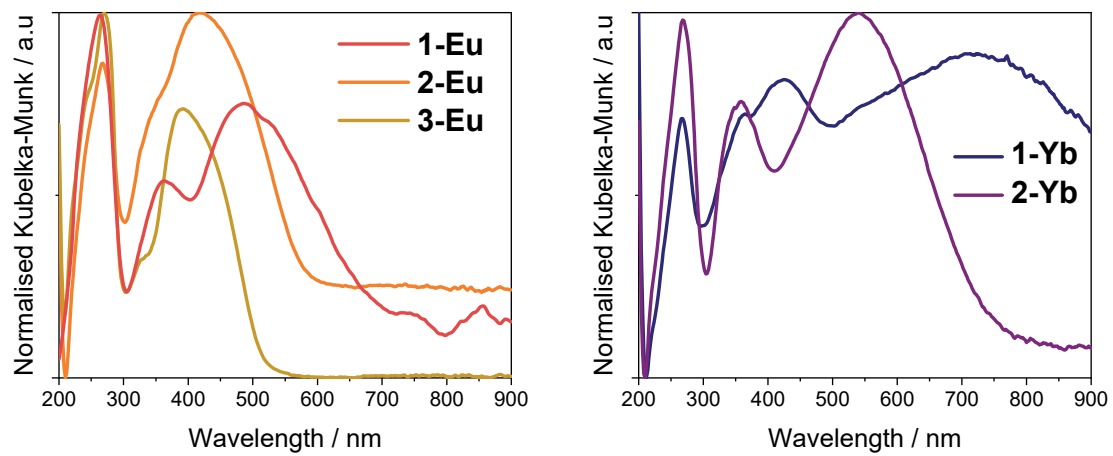


Fig. S11 Solid-state absorption profiles generated from diffuse reflectance measurements using the Kubelka–Munk equation ($k/s = (1 - R)^2/2R$; k = molar absorption coefficient, s = scattering coefficient, R = absolute reflectance of the sample).

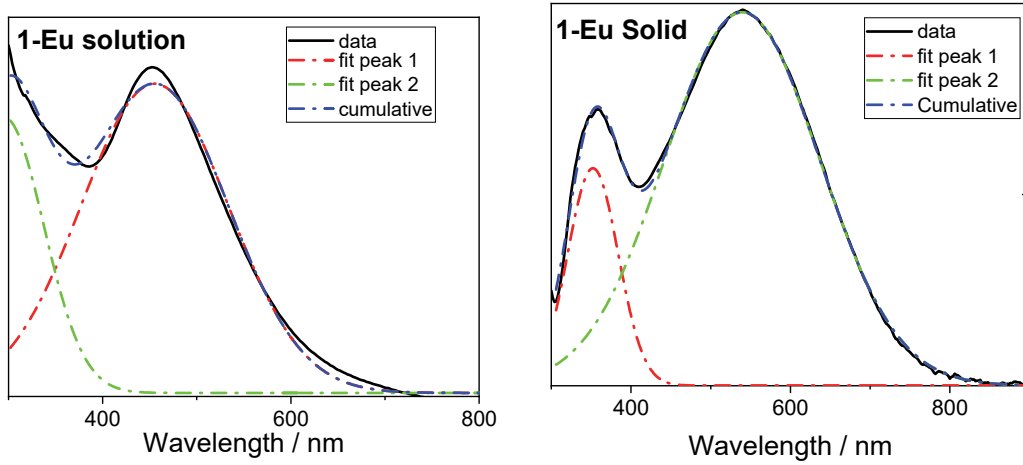


Fig. S12 Solution (MeCN) and solid-state ($\sim 5\%$ KBr) absorption spectra (UV-Vis region)
for **1-Eu** with 2 peak Gaussian fit (R^2 solution = 0.995; R^2 solid = 0.999)

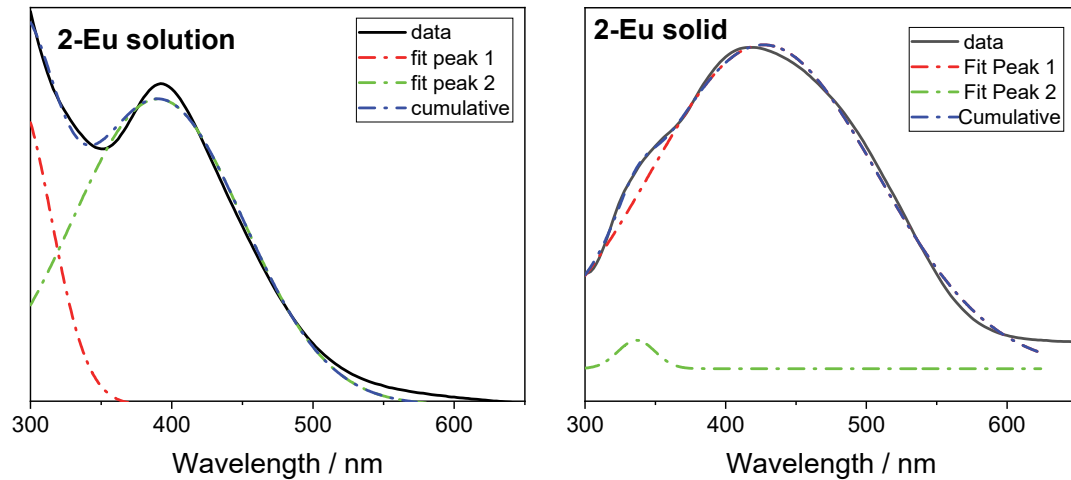


Fig. S13 Solution (MeCN) and solid-state ($\sim 5\%$ KBr) absorption spectra (UV-Vis region)
for **2-Eu** with 2 peak Gaussian fit (R^2 solution = 0.997; R^2 solid = 0.997)

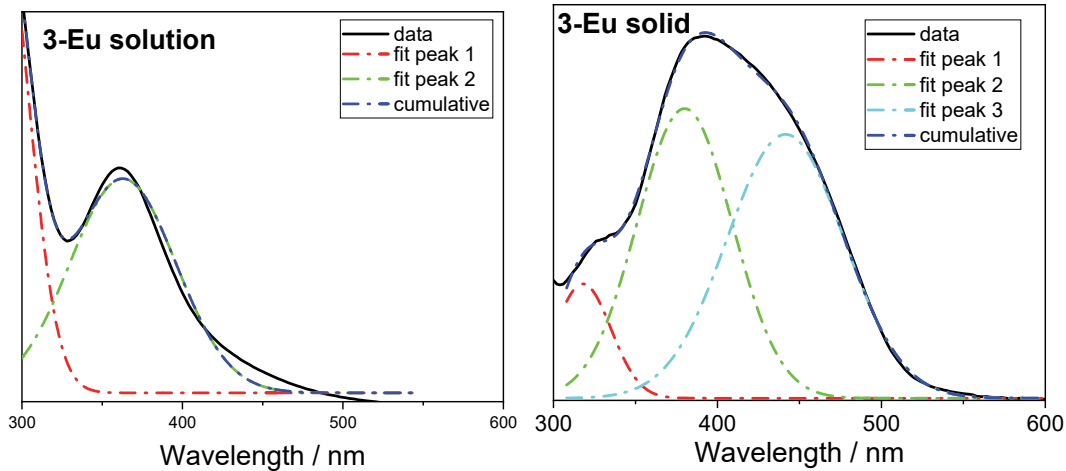


Fig. S14 Solution (MeCN) and solid-state ($\sim 5\%$ KBr) absorption spectra (UV-Vis region) for **3-Eu** with 2 peak Gaussian fit for solution ($R^2 = 0.991$) and 3 peak Gaussian fit for solid ($R^2 = 0.999$)

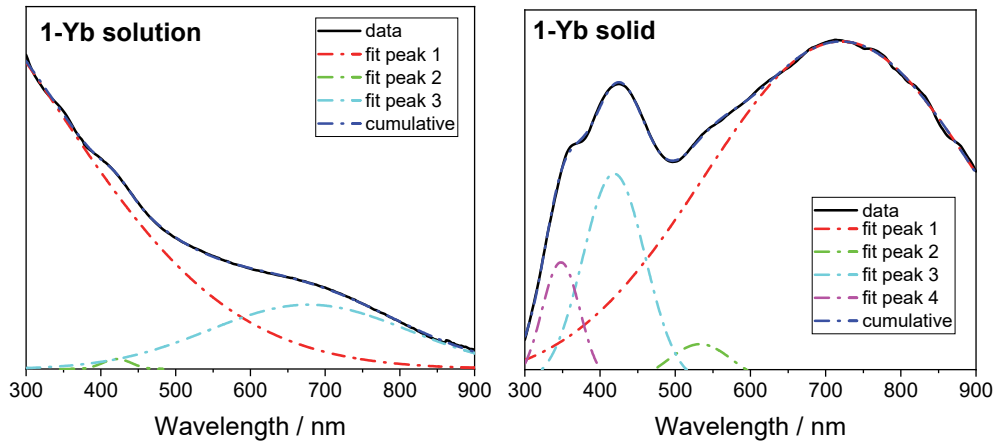


Fig. S15 Solution (MeCN) and solid-state ($\sim 5\%$ KBr) absorption spectra (UV-Vis region) for **1-Yb** with 3 peak Gaussian fit for solution ($R^2 = 0.999$) and 4 peak Gaussian fit for solid ($R^2 = 0.998$)

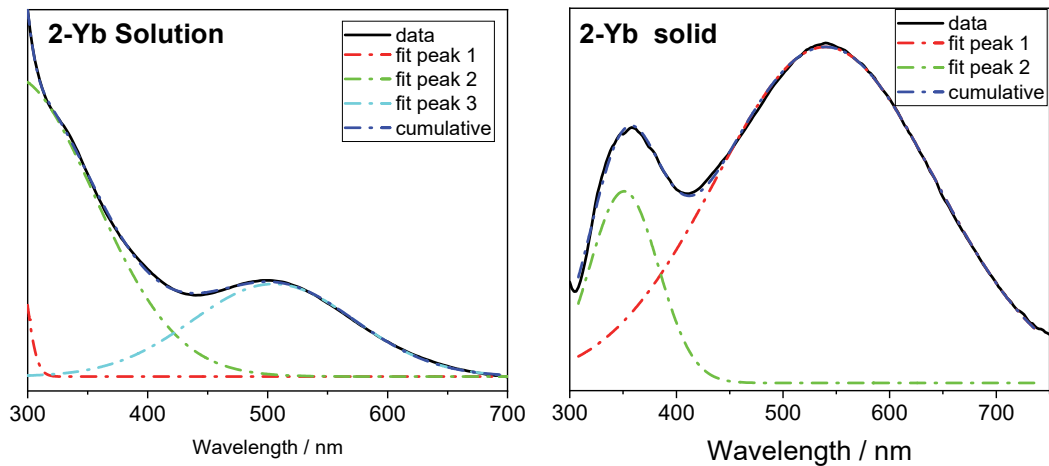


Fig. S16 Solution (MeCN) and solid-state ($\sim 5\%$ KBr) absorption spectra (UV-Vis region) for **2-Yb** with 3 peak Gaussian fit for solution ($R^2 = 0.999$) and 2 peak Gaussian fit for solid ($R^2 = 0.998$)

Table S4 Summary of the results from fitting electronic spectra of **1-Ln**, **2-Ln** and **3-Ln** to a multi-peak gaussian function

Compound	Solution		Solid	
	λ_{max} (nm)	FWHM (nm)	λ_{max} (nm)	FWHM (nm)
1-Eu	295 (± 3)	100 (± 6)	352 (± 1)	75 (± 1)
	455 (± 1)	184 (± 2)	539 (± 1)	229 (± 1)
2-Eu	289 (± 4)	61 (± 5)	337 (± 1)	31 (± 4)
	390 (± 1)	142 (± 2)	427 (± 1)	189 (± 2)
3-Eu	286 (± 4)	42 (± 4)	318 (± 1)	40 (± 1)
	363 (± 1)	78 (± 1)	380 (± 1)	68 (± 1)
			442 (± 1)	84 (± 1)
1-Yb	341 (± 1)	163 (± 4)	348 (± 1)	60 (± 1)
	421 (± 0.9)	46 (± 2)	419 (± 1)	97 (± 2)
	678 (± 3)	313 (± 7)	533 (± 2)	100 (± 4)
			721 (± 1)	428 (± 4)
2-Yb	286 (± 2)	162 (± 3)	351 (± 1)	76 (± 1)
	505 (± 1)	159 (± 2)	540 (± 1)	242 (± 2)

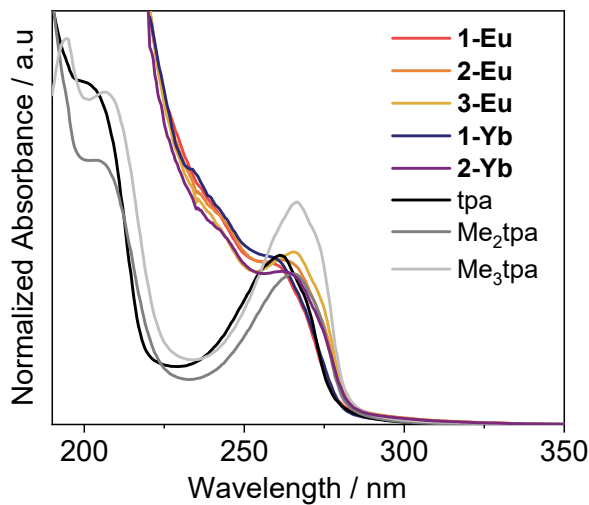


Fig. S17 Normalized UV absorption spectra for MeCN solutions of compounds **1-Ln**, **2-Ln**, and **3-Ln** versus the free ligands (tpa, Me₂tpa, Me₃tpa).

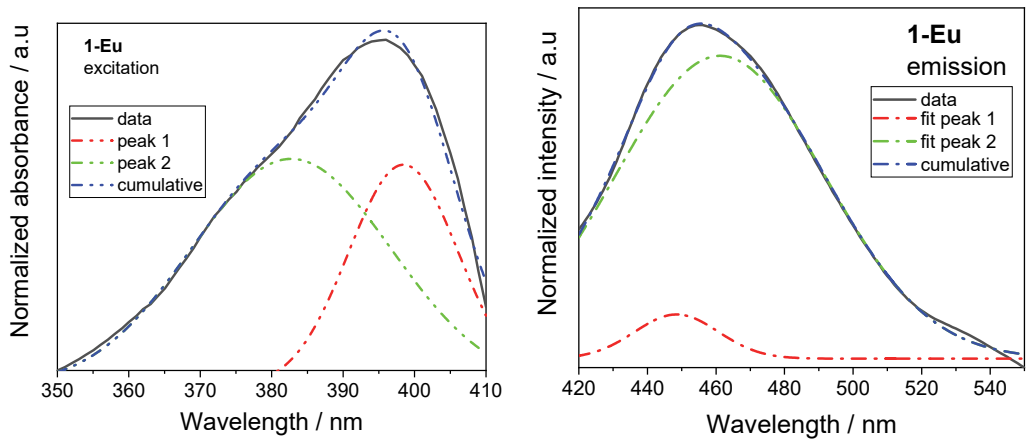


Fig. S18 Solution excitation (left) and emission (right) spectra for **1-Eu** with 2 peak Gaussian fit ($R^2_{\text{exc}} = 0.993$; $R^2_{\text{em}} = 0.999$)

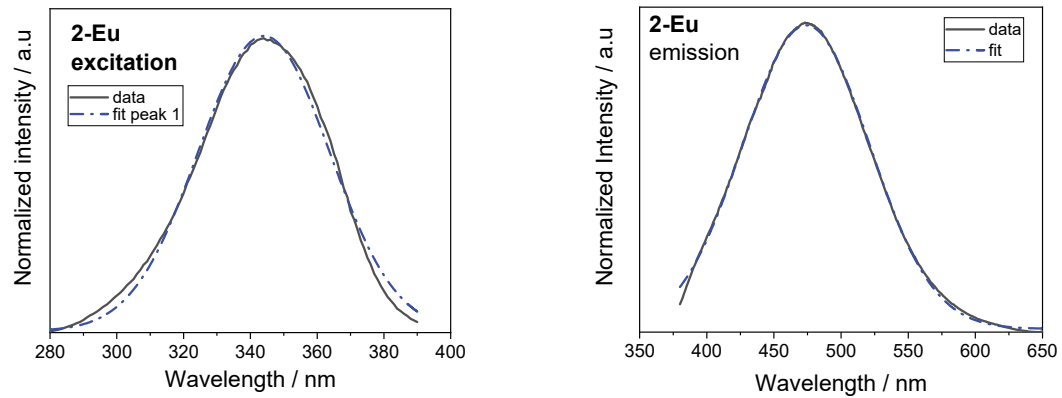


Fig. S19 Solution excitation (left) and emission (right) spectra for **2-Eu** with 2 peak and 1 peak Gaussian fit, respectively ($R^2_{\text{exc}} = 0.996$; $R^2_{\text{em}} = 0.999$). It was also possible to fit the excitation to a single maximum considering data between 250 and 400 nm.

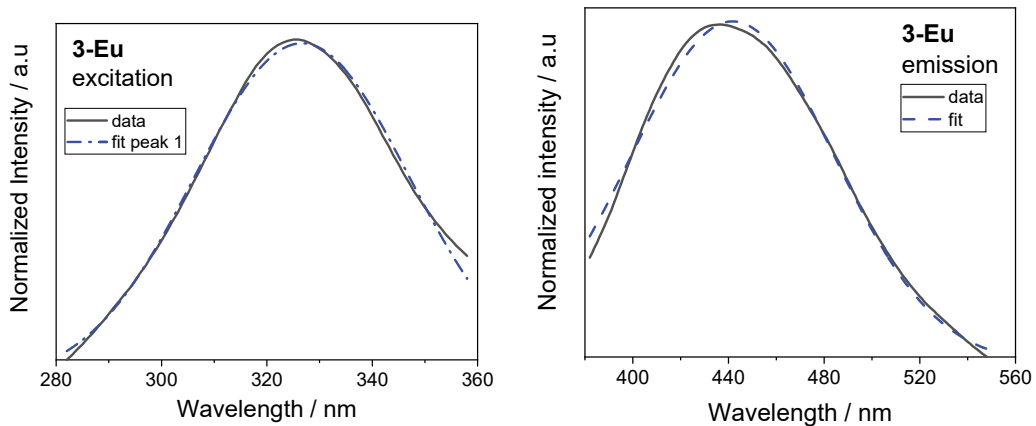


Fig. S20 Solution excitation and emission spectra for **3-Eu** with Gaussian fit ($R^2_{\text{exc}} = 0.996$; $R^2_{\text{em}} = 0.995$)

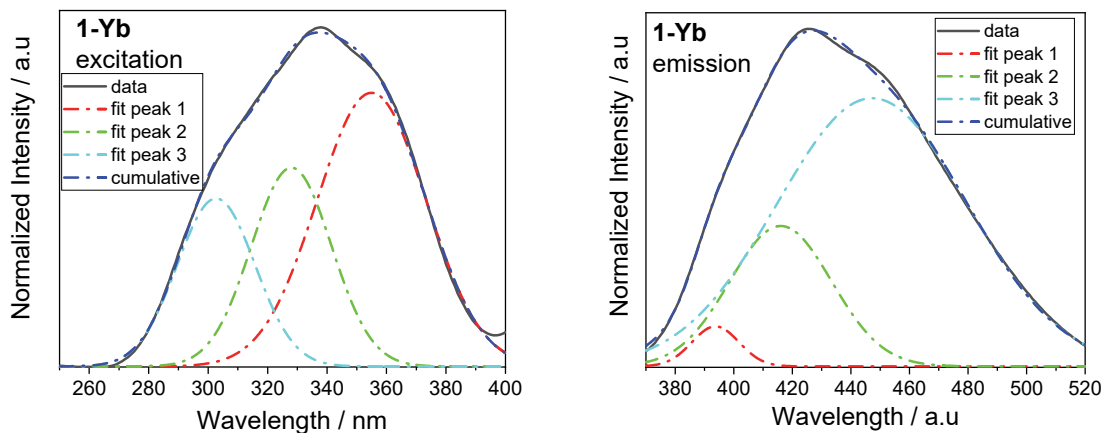


Fig. S21 Solution excitation and emission spectra for **1-Yb** with 1 peak Gaussian fit ($R^2_{\text{exc}} = 0.999$; $R^2_{\text{em}} = 0.995$). Despite the asymmetry of the peaks, it was not possible to obtain a converged fit considering 2 or more maxima.

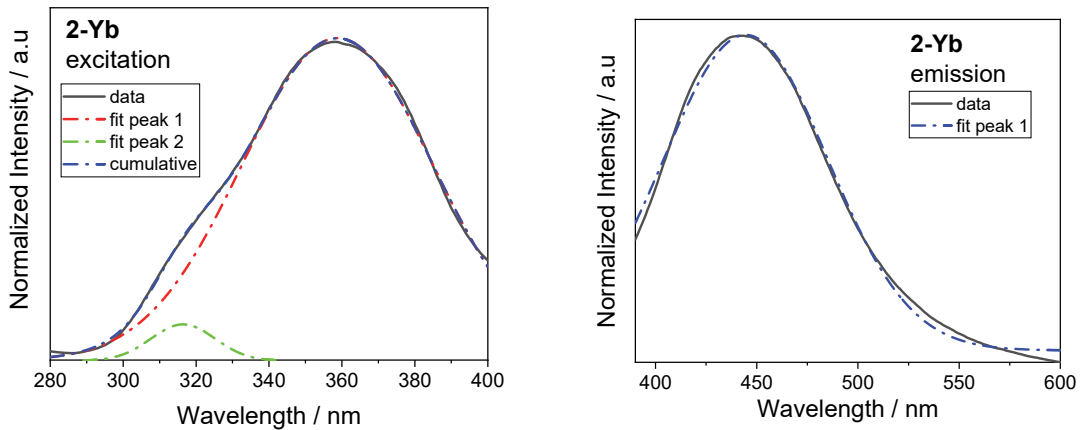


Fig. S22 Solution excitation and emission spectra for **2-Yb** with 2 peak and 1 peak Gaussian fit, respectively ($R^2_{\text{exc}} = 0.999$; $R^2_{\text{em}} = 0.997$).

Table S5 Summary of the results from fitting excitation and emission spectra for **1-Ln**, **2-Ln** and **3-Ln** (2 mM in MeCN) to multi-peak gaussian function.

Compound	Excitation		Emission		Stokes
	Position (nm)	FWHM (nm)	Position (nm)	FWHM (nm)	Shift (nm)
1-Eu	383 (± 4)	33 (± 6)	449 (± 1)	29 (± 2)	66
	398 (± 1)	18 (± 2)	461 (± 1)	72 (± 1)	63
2-Eu	344 (± 1)	46 (± 1)	474 (± 1)	111 (± 1)	130
3-Eu	327 (± 1)	48 (± 1)	442 (± 1)	100 (± 1)	115
1-Yb	303 (± 2)	31 (± 2)	394 (± 1)	19 (± 2)	91
	328 (± 1)	32 (± 3)	416 (± 1)	41 (± 2)	88
	355 (± 2)	43 (± 2)	447 (± 2)	76 (± 2)	92
2-Yb	316 (± 1)	21 (± 1)			
	359 (± 1)	68 (± 1)	445 (± 1)	95 (± 1)	86

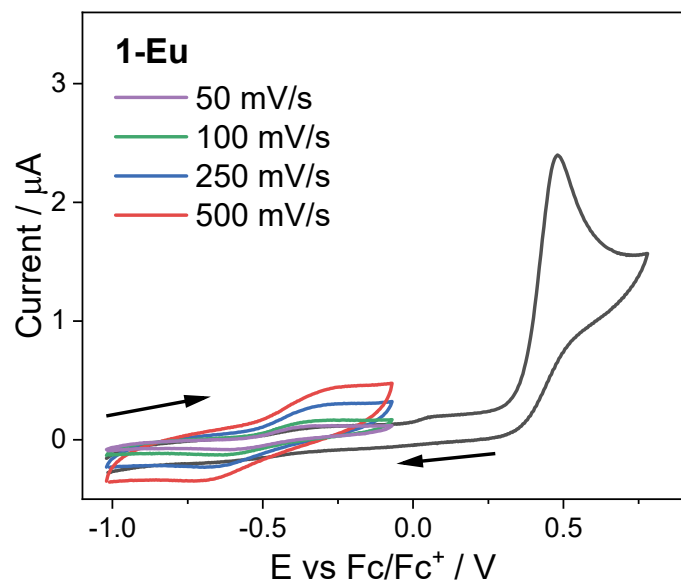


Fig. S23 Cyclic voltammograms of **1-Eu** (0.5 mM in MeCN; 0.25 M TBAPF₆) with scan rate dependence of first oxidation.

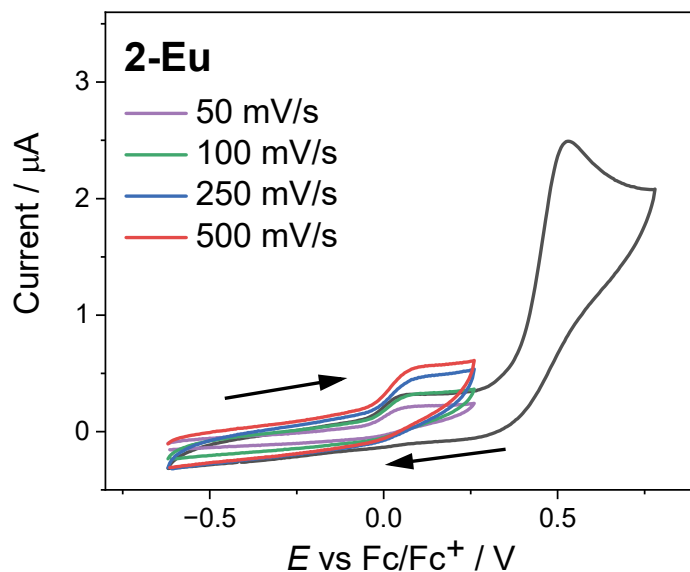


Fig. S24 Cyclic voltammograms of **2-Eu** (0.5 mM in MeCN; 0.25 M TBAPF₆) with scan rate dependence of first oxidation.

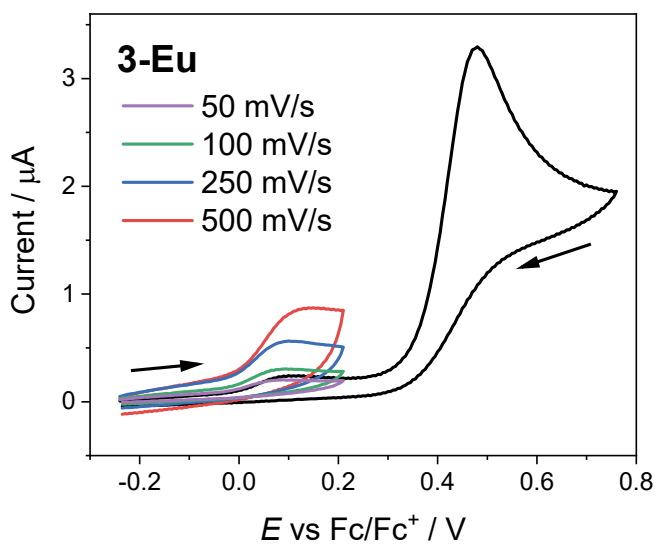


Fig. S25 Cyclic voltammograms of **3-Eu** (0.5 mM in MeCN; 0.25 M TBAPF₆) with scan rate dependence of first oxidation.

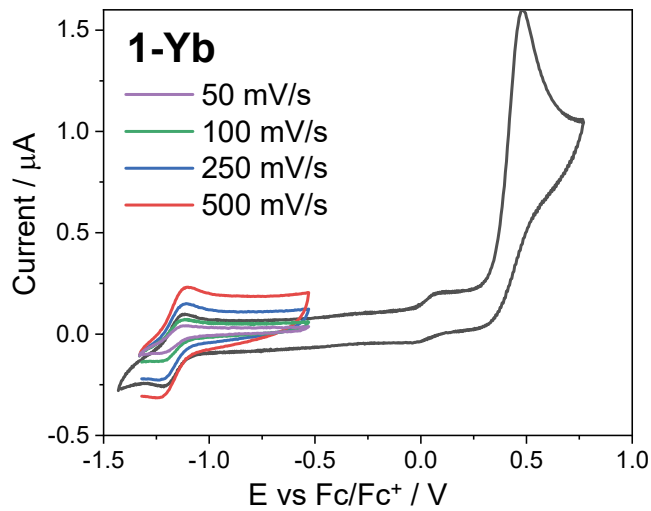


Fig. S26 Cyclic voltammograms of **1-Yb** (0.5 mM in MeCN; 0.25 M TBAPF₆) with scan rate dependence of first oxidation.

References

- 1 M. Pinsky and D. Avnir, *Inorg. Chem.*, 1998, **37**, 5575–5582.
- 2 D. Casanova, J. Cirera, M. Llunell, P. Alemany, D. Avnir and S. Alvarez, *J. Am. Chem. Soc.*, 2004, **126**, 1755–1763.